IEEE Access
Multidisciplinary ⋮ Rapid Review ⋮ Open Access Journal

Received 1 October 2025, accepted 19 November 2025, date of publication 26 November 2025,
date of current version 18 December 2025.

Digital Object Identifier 10.1109/ACCESS.2025.3637238

RESEARCH ARTICLE

Design of a Wrapped Rib Mesh Reflector Antenna With a Precise Parabolic Surface and High Volume-Reduction Efficiency Using a Lightweight and Simple Mechanical Configuration

EN-YEAL YIM, CHANGHYEON IM, AND HOSUNG CHOO, (Senior Member, IEEE)
Department of Electronic and Electrical Engineering, Hongik University, Seoul 04066, South Korea

Corresponding author: Changhyeon Im (b615171@mail.hongik.ac.kr)

This work was supported by Korea Research Institute for Defense Technology Planning and Advancement (KRIT) grant funded by Korean Government, Defense Acquisition Program Administration (DAPA), Space Signal Intelligence Research Laboratory, in 2022, under Grant KRIT-CT-22-021.

ABSTRACT In this paper, we propose a wrapped rib mesh reflector antenna with spring hinges and column stoppers for a high precision reflector surface. To achieve a high precision surface, twelve spring hinges and column stoppers are employed on the center hub, and curved ribs are connected to each spring hinge. The curved ribs are designed based on the parabola equation and are made of Carbon Fiber Reinforced Plastic (CFRP), which has both high elasticity and flexibility, enabling the ribs to be wrapped into a compact circular shape around the center hub. A conducting mesh with high reflectivity is attached to the upper surface of the deployable structure. In this configuration, the mesh can form a parabolic shape consistent with the parabola equation used in the design of the curved ribs. Therefore, the proposed mesh reflector can form a high precision reflector surface. Moreover, when the reflector is stowed in the rocket payload, the diameter of the reflector is reduced from 1.5 m to 0.2 m, and the height is maintained at 0.26 m. This means that the fabricated model has a deployment volume of 0.585 m^3 (1.5 m × 1.5 m × 0.26 m) and a stowed volume of 0.0104 m^3 (0.2 m × 0.2 m × 0.26 m), thus achieving a volume-reduction efficiency of 98.22%. To verify the electrical characteristics of the proposed antenna, the bore-sight gain of the proposed antenna is measured in the far-field environment. The measured average bore-sight gain and aperture efficiency from 2 GHz to 6 GHz are 27.4 dBi and 18.1%, respectively, which agrees well with the simulated results of 26.7 dBi and 14.4%. These results show a 4.4 dB decrease compared to the average bore-sight gain (31.8 dBi) when using a gold-coated molybdenum mesh with 97% reflectivity.

INDEX TERMS Reflector antennas, mesh antennas, deployable antennas, satellite antennas.

I. INTRODUCTION

Recently, wide-area communication systems have been utilized to support communication across diverse environments, including urban areas, mountainous regions, oceans, and polar regions [1], [2], [3]. In conventional communication systems, base-station antennas are typically used for wide-area communication [4], [5], [6]. However, base-station antennas have limitations in Line-Of-Sight (LOS) due to terrain and obstacles, which can restrict communication coverage [7]. To overcome LOS limitations, research on satellite communication systems has been actively conducted [8], [9], [10]. These satellite systems typically operate at altitudes ranging from 200 km to 36,000 km above the Earth's surface [11]. Therefore, satellite systems should transmit and receive data over long distances from Earth. To achieve the received power requirements at high altitudes, high-gain antennas are necessary for satellite systems. Phased array

The associate editor coordinating the review of this manuscript and approving it for publication was Lei Zhao.

antennas [12] and large-diameter reflector antennas [13] are generally used as communication antennas for this purpose. As is well known, increasing the aperture size of phased array antennas and reflector antennas results in a higher gain. As the aperture size of the phased array antennas increases, the size and weight of a Transmit/Receive Module (TRM) also increase. Consequently, it becomes unsuitable for stowing in a rocket payload due to volume and weight limitations [14]. On the other hand, reflector antennas have a simple design consisting of a parabolic reflector and feeder antennas. Moreover, they can achieve high-gain simply by increasing the reflector diameter without additional components. As the diameter of the reflector increases, its volume and weight also increase, which limits any further expansion of the reflector diameter. Therefore, to stow a large-diameter reflector within the limited payload space, it is necessary to develop methods for reducing its weight and stowed volume. To solve this issue, research has been conducted on deployable mesh reflectors, which feature lightweight properties and reduced stowed volume [15]. Deployable mesh reflector antennas have been designed with various deployment mechanisms, such as folded rib mesh reflectors [16], [17], [18], truss structure mesh reflectors [19], [20], and inflatable mesh reflectors [21]. These reflector antennas have the advantage of reducing the stowed volume; however, each type also has its disadvantages. For example, the folded rib mesh reflectors increase the height of the stowed shape, while the truss structure mesh reflectors involve complex mechanical configurations, and the inflatable mesh reflectors may form an inaccurate parabolic surface due to external shocks and thermal effects. To address these problems, research of wrapped rib mesh reflector antennas, which can achieve high volume-reduction efficiency through a simple mechanical configuration, has been conducted [22], [23]. In these wrapped rib reflector antennas, ribs are arranged tangentially to the center hub, then the mesh reflector cannot form the precise parabolic surface using a simple parabola equation. Thus, to form the precise parabolic surface in the wrapped rib mesh reflector, the equation that considers a center hub's diameter, number of ribs, and interval between each rib should be applied to the curved ribs, making the design process of the reflector more complex. Moreover, when the deployed ribs are over-rotated, a surface deformation occurs, leading to electrical performance degradation. Therefore, the mechanical configuration, which can adjust and constrain the direction of deployed ribs, is required for the wrapped rib mesh reflector design.

In this paper, we propose a wrapped rib mesh reflector antenna with spring hinges and column stoppers for a high precision reflector surface. To achieve a high precision surface, twelve spring hinges and column stoppers are employed on the center hub, and curved ribs are connected to each spring hinge. The curved ribs are designed based on the parabola equation and are made of Carbon Fiber Reinforced Plastic (CFRP), which has light weight, high elasticity, and flexibility [24], enabling the ribs to be wrapped into a compact circular shape around the center hub. As a result, the reflector achieves high volume-reduction efficiency through a light and simple mechanical configuration, making it suitable for stowing in a rocket payload. For a lightweight and compact stowed volume, a conducting mesh with high reflectivity is attached to the upper surface of the deployable structure. When the satellite reaches its operating altitude, the wrapped ribs automatically deploy due to the elasticity of the CFRP and the spring hinges, resulting in the attached mesh reforming into a parabolic shape. During deployment, the ribs are constrained by the column stopper, arranging them perpendicular to the center hub. This deployment structure differs from conventional wrapped rib reflectors, in which the ribs are arranged tangentially to the center hub. In conventional structures, forming the precision reflector surface is more challenging because their curvature does not conform to the parabola equation. In contrast, due to the spring hinges and column stoppers, the mesh of the proposed antenna can form a parabolic shape consistent with the parabola equation used in the design of the curved ribs. Therefore, the proposed mesh reflector has a high precision reflector surface. The proposed reflector is optimized using the CST Studio Suite full EM simulator [25], and it is fabricated to verify its mechanical properties and electrical performance. This fabricated model has a deployment volume of 0.585 m^3(1.5 m × 1.5 m × 0.26 m) and a stowed volume of 0.0104 m^3(0.2 m × 0.2 m × 0.26 m), meaning it achieves a volume-reduction efficiency of 98.22%. The average measurement bore-sight gain is 27.4 dBi from 2 GHz to 6 GHz, with an average aperture efficiency of 18.1%, which agrees well with the simulation results.

II. DESIGN OF THE WRAPPED RIB MESH REFLECTOR ANTENNA

A. DESIGN OF THE PROPOSED ANTENNA

Figure 1 illustrates the geometry of the proposed wrapped rib mesh reflector antenna with spring hinges and column stoppers for a high precision reflector surface. As shown in Figure 1(a), the proposed mesh reflector is assembled from multiple curved ribs (N_r), conducting mesh, and a center hub. For high-gain characteristics, the proposed antenna is designed with the deployed diameter (D_1) of 1.5 m. Considering both stowed volume and feeder distance, the proposed reflector's focal ratio (F/D) and height (h_1) are determined to be 0.5 and 0.26 m, respectively. To achieve a high precision surface, twelve spring hinges and column stoppers are employed on the center hub, and curved ribs are connected to each spring hinge. The curved ribs are designed based on the parabola equation and are made of CFRP, which has both high elasticity and flexibility. As a result, the CFRP ribs can be wrapped and returned to their original shape. Using this characteristic, each rib can be wrapped around the center hub when the reflector is stowed in the rocket payload and returned to its deployed shape at the operating altitude. For

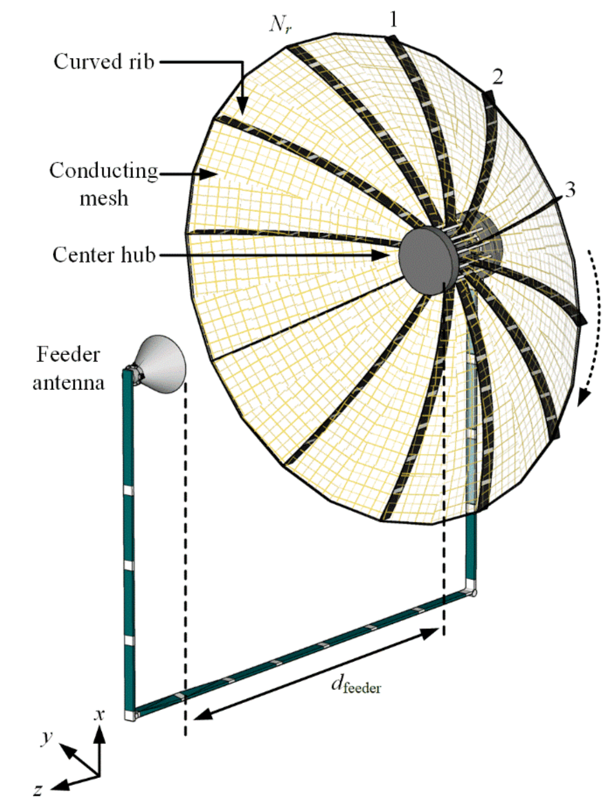

(a)

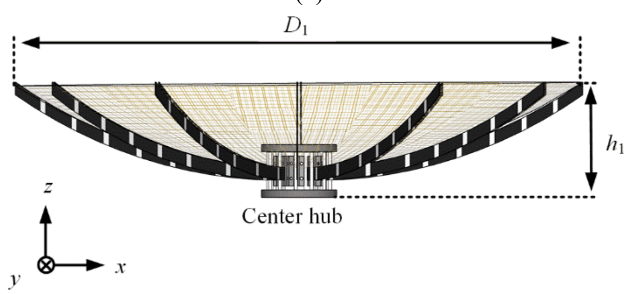

(b)

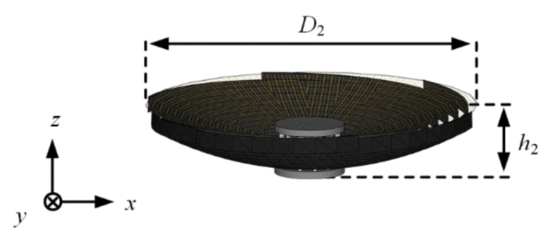

(c)

FIGURE 1. Geometry of the proposed antenna element. (a) Isometric view of the deployed shape. (b) Side view of the deployed shape. (c) Side view of stowed shape.

a lightweight and compact stowed volume, the conducting mesh with a reflectivity of 97% is applied as the reflector surface. As shown in Figures 1(b) and 1(c), when the reflector is stowed in the rocket payload, the diameter of the reflector is reduced from D_1 to D_2, and the height is maintained at h_2, which is the same as the deployed shape's height of h_1. This indicates that the proposed antenna achieves a high volume-reduction efficiency, making it suitable for stowing in a rocket payload. During deployment, the wrapped ribs automatically deploy due to the elasticity of the CFRP and spring hinges. Once deployed, they are constrained by the column stoppers, arranging them perpendicular to the center hub. In this configuration, the spring hinges and column stoppers enable the mesh to form a high precision reflector surface. To optimize the proposed antenna, the proposed antenna is modeled and analyzed using EM simulator CST. Using this simulator, the number of ribs (N_r) is optimized to be 12 considering both the mechanical and electrical performance. For maximum aperture efficiency, the optimum feeder distance (d_{feeder}) is also obtained as 0.725 m in this simulator, in which aperture efficiency increases to 39.7%. To verify the feasibility of the proposed antenna, the proposed antenna is fabricated, and the performance, such as radiation pattern, bore-sight gain, and aperture efficiency is measured. Moreover, to investigate the mechanical performance of the proposed antenna, the deployment test is conducted on the fabricated antenna. During the deployment test, the stowed diameter (D_2) and height (h_2) are observed to be 0.2 m and 0.26 m, respectively. Detailed design parameters are listed in Table 1.

TABLE 1. Design parameters of the proposed antenna.

Parameters	Descriptions	Values
D_1	Deployed diameter	1.5 m
D_2	Stowed diameter	0.2 m
N_r	Number of ribs	12
d_{feeder}	Feeder distance	0.725 m
h_1	Deployed height	0.26 m
h_2	Stowed height	0.26 m

Figure 2 illustrates the mechanical components of the proposed wrapped rib mesh reflector antenna. As shown in Figure 2(a), the curved CFRP ribs are designed based on a parabola equation. To reduce the weight of the reflector, the curved ribs adopt a tapered shape, where the height of the curved rib gradually decreases from h_{root} to h_{tip}. Figure 2(b) shows the top view of the curved rib. Each curved rib has a length of l and a thickness of t, providing the flexibility needed to enable the ribs to be wrapped into a compact circular shape and the elasticity required for automatic deployment. Moreover, the CFRP curved ribs have high thermal durability against thermal effects in satellite orbit [26], [27]. Figure 2(c) presents the isometric view of the center hub. The center hub, which is made of lightweight and durable resin, contains a top hub part, a bottom hub part, and twelve inner hub parts. Each inner hub part incorporates a spring hinge that connects it to the curved rib, while the bottom hub part has twelve column stoppers that prevent any over-rotation of the spring hinges. The role of the column stoppers can be explained more clearly through the

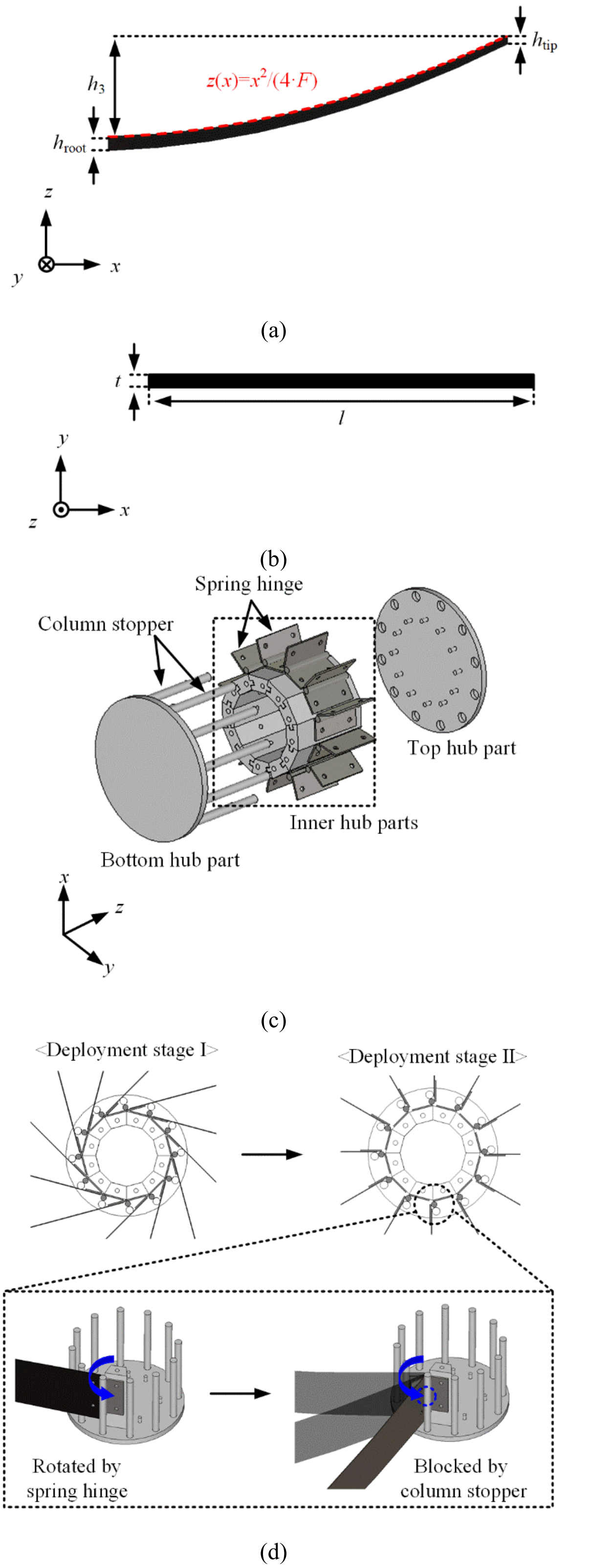

FIGURE 2. **Mechanical components of the proposed antenna. (a) Side view of the curved rib. (b) Top view of the curved rib. (c) Isometric view of the center hub. (d) Deployment mechanism of the center hub.**

process of a two-stage deployment, as shown in Figure 2(d). In deployment stage I, the wrapped ribs automatically deploy, following the conventional mechanism employed in typical wrapped rib reflectors. In stage II, the spring hinges rotate the ribs using the restoring force of the springs. The column stoppers then constrain the ribs, ensuring they are aligned perpendicular to the center hub. Thus, the ribs are arranged tangentially to the center hub, and the mesh can form a parabolic shape consistent with the parabola equation used in the design of the curved ribs. Therefore, the proposed mesh reflector has a high precision reflector surface. The detailed geometrical parameters of the mechanical components are listed in Table 2.

TABLE 2. **Design parameters of the mechanical component.**

Parameters	Descriptions	Values
h_3	Height of rib	0.1875 m
h_{root}	Height of root	50 cm
h_{tip}	Height of tip	30 cm
t	Thickness of rib	0.5 mm
l	Length of rib	700 mm

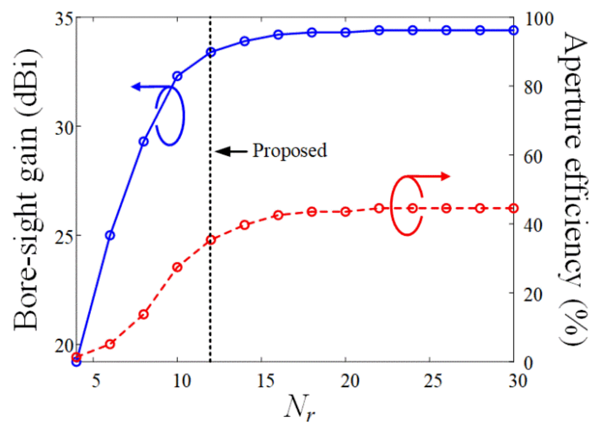

FIGURE 3. **Bore-sight gain and aperture efficiency of the proposed reflector antenna in accordance with N_r at 5 GHz.**

B. ELETRICAL ANALYSIS OF THE PROPOSED ANTENNA

Since the mesh cannot maintain a specific shape on its own, the proposed antenna preserves the shape of the reflector surface by attaching it to the curved rib. The attached mesh is stretched by the tension exerted by the ribs on both sides, resulting in a flat mesh surface between each pair of ribs. This results in a surface deformation relative to the ideal reflector surface, leading to a degradation in the performance of the reflector antenna. One approach to reducing surface deformation is to increase the number of ribs; however, this increases the reflector's weight, stowed volume, and mechanical complexity. Therefore, it is important to determine the appropriate number of ribs (N_r) based on design requirements. Figure 3 presents the bore-sight gain and aperture efficiency of the proposed mesh reflector antenna in accordance with N_r at 5 GHz. As N_r increases from 4 to 30, the bore-sight gain increases from 19.2 dBi to 34.4 dBi, while the aperture efficiency increases from 1.35% to 44.5%. In consideration of both

TABLE 3. Comparison Table with previous research.

Reflector	Diameter	Mechanical components	Bore-sight gain	Aperture efficiency	Volume-reduction efficiency	Mass (mass per volume)
[16]	1.0 m	Ribs: 24 Joints: 48	31.6 dBi @ 10 GHz	13.5%	75.7%	-
[17]	0.5 m	Ribs: 30 Joints: 60	42.6 dBi @ 35.75 GHz	52.0%	90.4%	-
[18]	6.0 m	Ribs: 28 Joints: 56	-	-	74.8%	-
[22]	3.6 m	Ribs: 16 Joints: -	30.6 dBi @ 1.275 GHz	40.0%	95.74%	15 kg (1.78 kg/m^3)
[23]	0.5 m	Ribs: 16 Joints: -	-	-	96.00%	0.57 kg (15.2 kg/m^3)
This work	1.5 m	Ribs: 12 Joints: -	33.9 dBi @ 5 GHz	39.7%	98.22%	0.9 kg (1.54 kg/m^3)

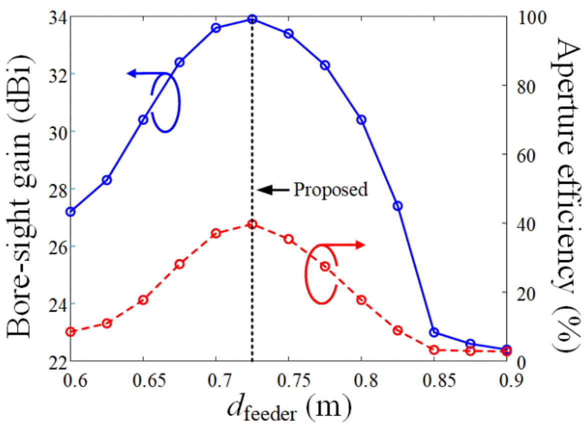

FIGURE 4. Bore-sight gain and aperture efficiency of the proposed reflector antenna in accordance with d_{feeder} at 5 GHz.

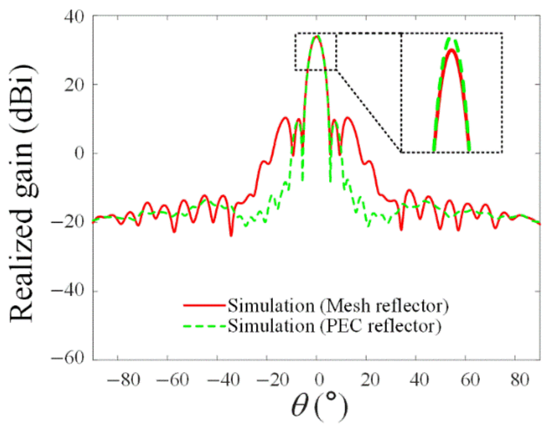

FIGURE 5. 2-D radiation patterns of the proposed antenna and PEC reflector antenna at 5 GHz.

electrical and mechanical performance, the proposed antenna design adopts $N_r = 12$, which results in a bore-sight gain of 32.3 dBi and an aperture efficiency of 35%.

To receive all reflected signals from the parabolic reflector with the same phase, the phase center of the feeder antenna should be located at the focal point (F) of the parabolic reflector [28]. Since the phase center is not located at the feeder's aperture, it is necessary to optimize the position of the feeder. Moreover, when the surface deformation is generated at the reflector surface, the focal point of the mesh reflector can shift [29]. Therefore, to maximize the aperture efficiency of the mesh reflector antenna, it is necessary to adjust d_{feeder} considering the phase center of the feeder antenna and the surface deformation of the mesh. Figure 4 shows the bore-sight gain and aperture efficiency of the proposed mesh reflector antenna in accordance with d_{feeder} at 5 GHz. To achieve maximum aperture efficiency, d_{feeder} is adjusted from 0.6 m to 0.9 m. When d_{feeder} is 0.75 m, which is the same value as the focal length F, the bore-sight gain and aperture efficiency are 32.3 dBi and 35%, respectively. By adjusting d_{feeder} to 0.725 m, the bore-sight gain and aperture efficiency are improved to 33.9 dBi and 39.7%, respectively.

Figure 5 presents the 2-D radiation patterns of the proposed antenna and a PEC reflector, both of which have a diameter of 1.5 m. The bore-sight gain of the proposed mesh reflector antenna is 33.9 dBi at 5 GHz, while the PEC reflector antenna has a gain of 35.5 dBi, indicating that the proposed antenna has a slightly lower gain performance. However, the PEC reflector antenna is unsuitable for limited payload environments due to its size and weight. In contrast, the proposed mesh reflector, with its lightweight and compact stowed shape, is more suitable for rocket payload stowing.

To confirm the feasibility of the proposed mesh reflector antenna, the number of mechanical components, bore-sight gain, aperture efficiency, volume-reduction efficiency, and mass are compared with those from previous studies [16], [17], [18], [22], [23], as shown in Table 3. In previous studies,

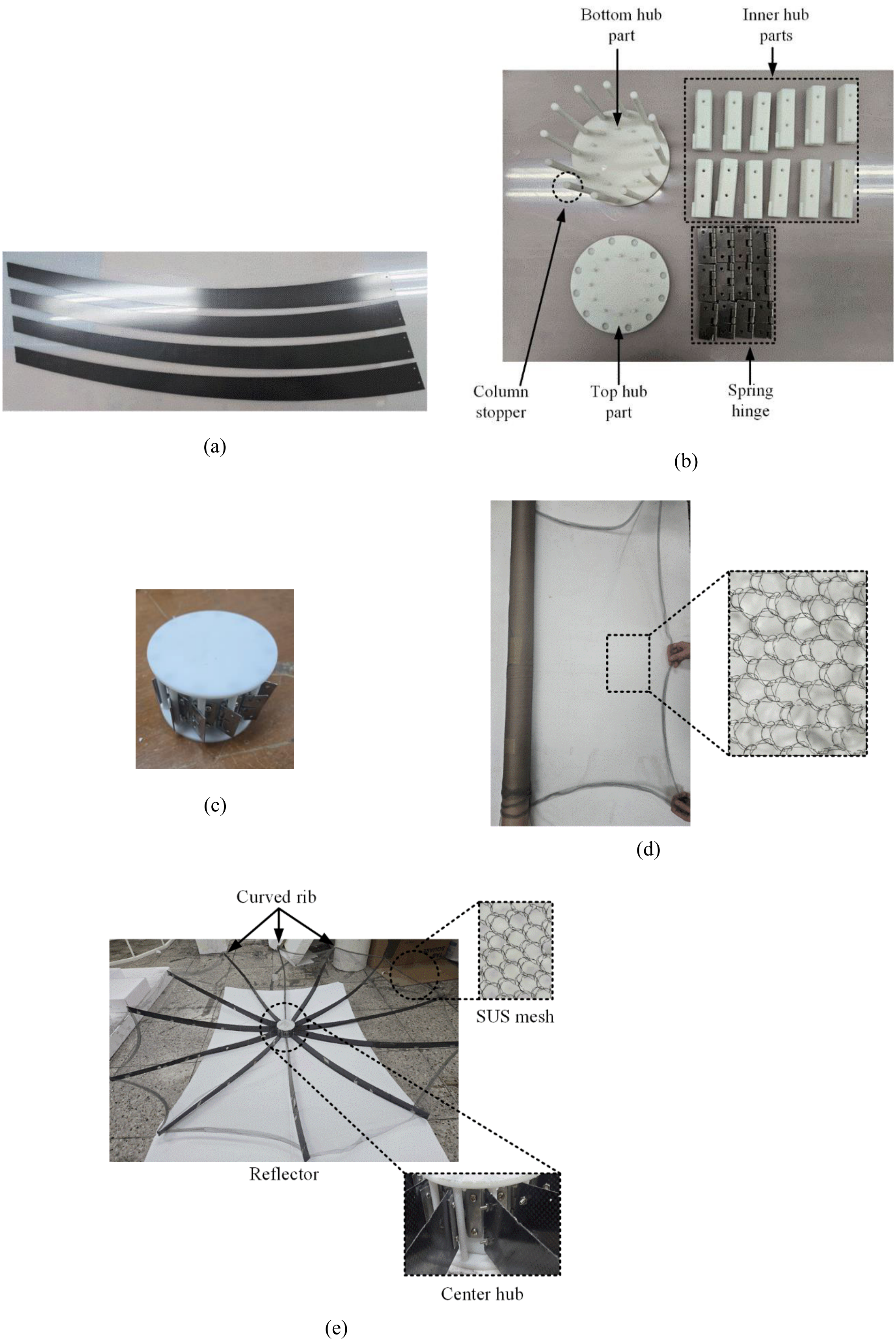

FIGURE 6. Photographs of the fabricated proposed antenna. (a) Curved ribs. (b) Each part of the center hub. (c) Fully assembled center hub. (d) SUS conducting mesh. (e) Fully assembled mesh reflector.

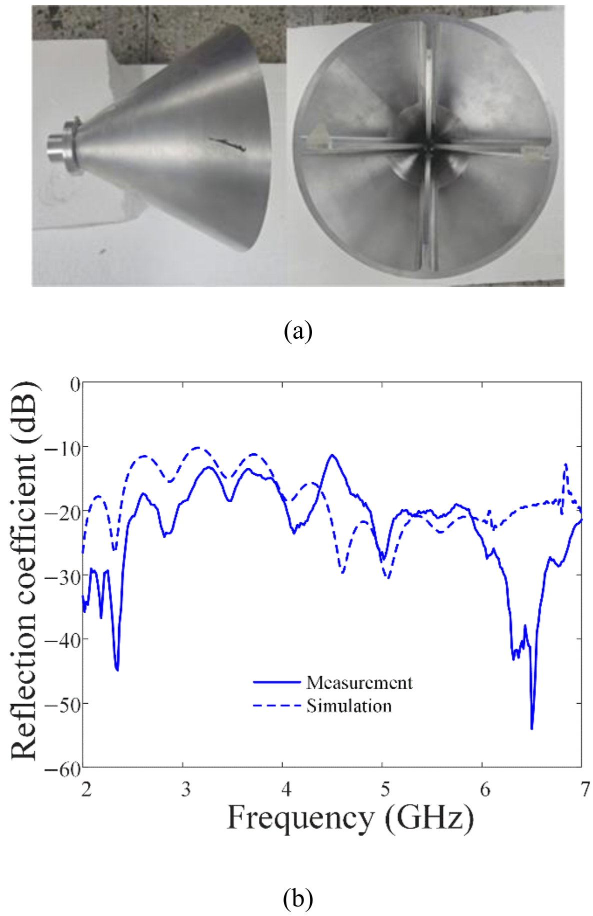

FIGURE 7. Reflection coefficient of the feeder antenna (a) Fabrication. (b) Reflection coefficient.

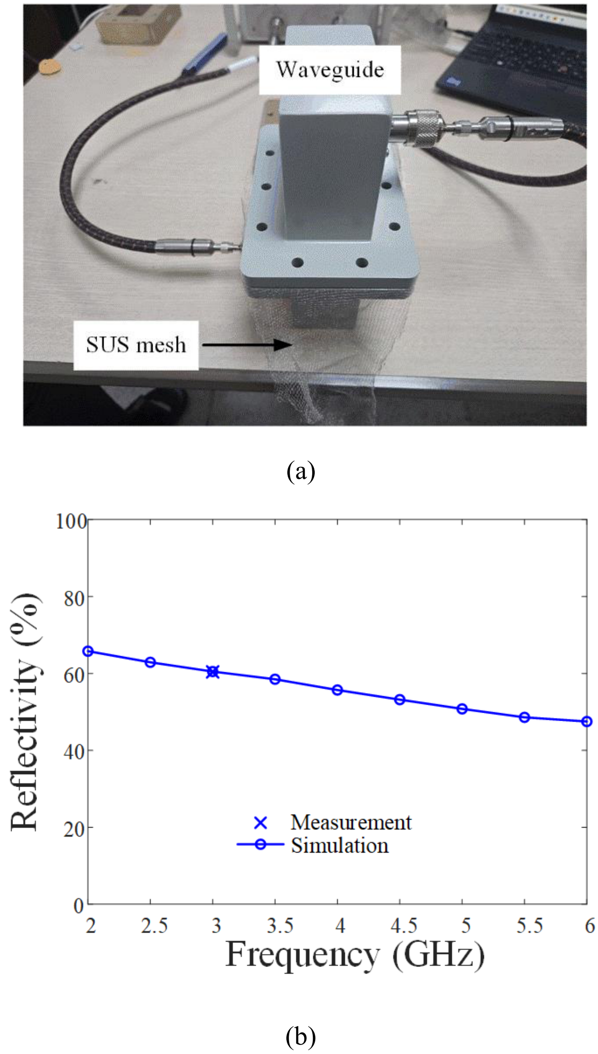

FIGURE 8. Reflectivity of the SUS mesh. (a) Measurement setup. (b) Reflectivity.

a multiple-joint structure has been adopted in the folded rib design to reduce the stowed volume of the reflector. In this configuration, the attached mesh is stretched by the tension exerted by the ribs and joints, creating a split flat surface between each pair of ribs. Since the split flat surface causes surface deformations, the number of ribs and joints should be increased to minimize these deformations. It also increases the reflector's weight, stowed volume, and mechanical complexity. In contrast, in our research, each curved rib is designed based on the parabola equation and is fabricated from a single piece of CFRP. As a result, there are no physically discrete parts within the ribs, which reduces surface deformation. Therefore, the proposed mesh reflector antenna achieves a high bore-sight gain of 33.9 dBi at 5 GHz and aperture efficiency of 39.7%, even though its design adopts $N_r = 12$, which is lower than that of other reflectors. In addition, the rib of the proposed antenna is made of CFRP, which has high elasticity and flexibility with lighter than spring steel used in the conventional wrapped rib mesh reflectors. Thus, the proposed antenna has a high volume-reduction efficiency of 98.22% using the lighter mechanical configuration, which has a lower mass per volume of 1.54 kg/m^3 than other wrapped rib mesh reflectors. This indicates that the proposed antenna is more suitable for stowing in a rocket payload than other wrapped rib mesh reflector antennas.

III. FABRICATION AND MEASUREMENT OF THE WRAPPED RIB MESH REFLECTOR ANTENNA

A. FABRICATION OF THE PROPOSED ANTENNA (SCALE-DOWN MODEL)

Figure 6 illustrates photographs of the fabricated antenna to verify its mechanical properties and electrical performance. Figure 6(a) shows the fabricated curved CFRP ribs, which are lightweight, high elasticity, and flexibility. Figure 6(b) presents individual parts of the center hub, which include the top hub part, bottom hub part, and twelve inner hub parts, all of which are made of lightweight and durable resin using a 3-D printing method. All parts are then sequentially assembled, and as shown in Figure 6(c). Each spring hinge is combined with each inner hub part to connect the curved rib and center hub, and column stoppers are printed in the bottom

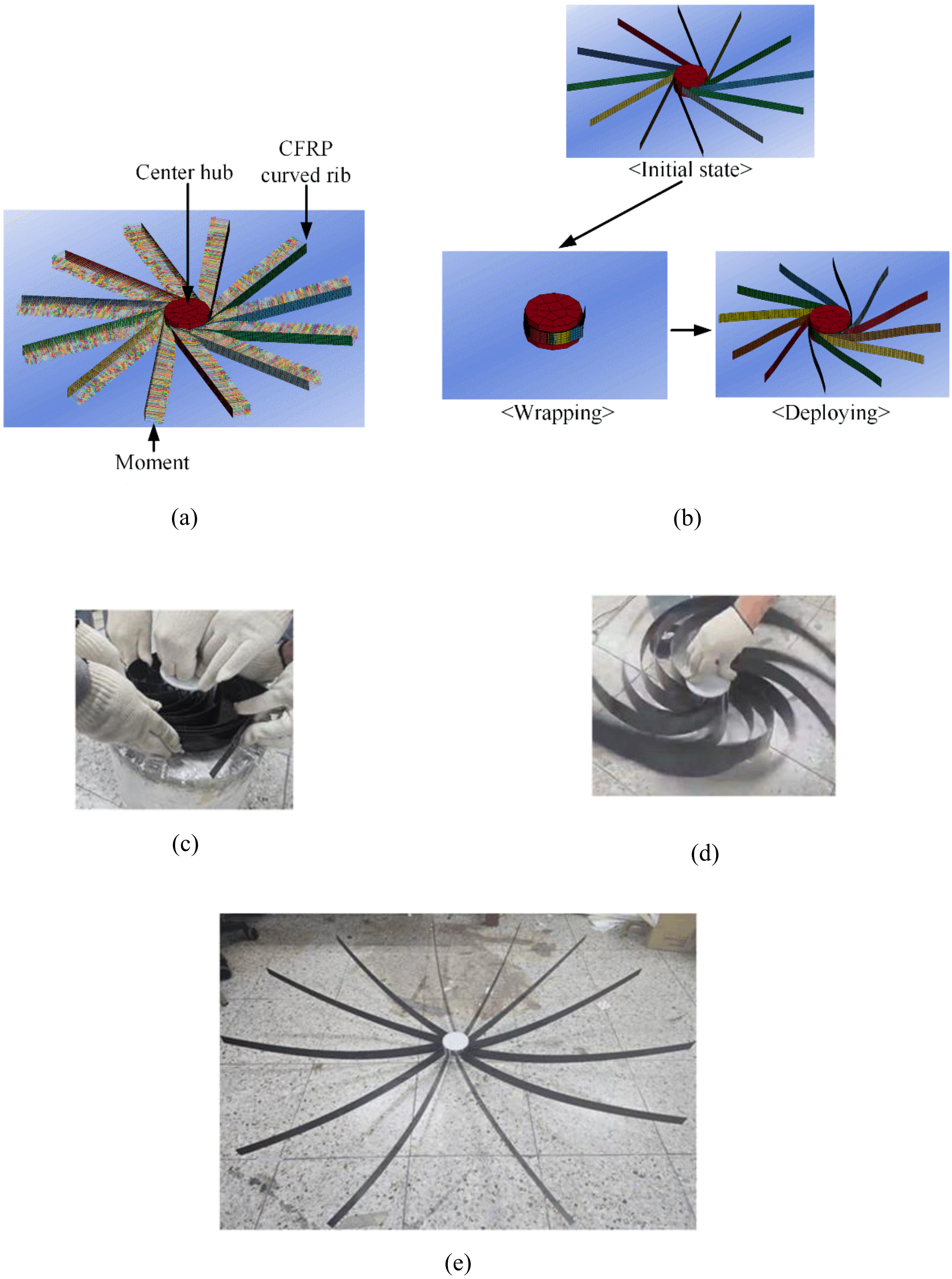

FIGURE 9. Deployment test of the proposed antenna. (a) Simulation setup of deployment. (b) Deployment process in simulation. (c) Stowed shape. (d) Intermediate shape. (e) Deployed shape.

hub part. Figure 6(d) shows a photograph of a Steel Use Stainless (SUS) mesh. To verify the feasibility, the proposed antenna is fabricated using a commercial conduction mesh. In this fabrication, we employ the SUS mesh (a reflectivity of 60.8% at 3 GHz) as the reflector surface instead of a gold-coated molybdenum mesh (a reflectivity of about 97% at 3 GHz) considering the manufacturing cost. The SUS mesh is then attached to the upper surface of the ribs, which enables it to function as a reflective surface, as shown in Figure 6(e).

For various communication systems, such as remote sensing and weather monitoring (S-band), geostationary satellite communications and data link transmissions (C-band), the proposed antenna should have a broadband characteristic [30]. The operating bandwidth of a reflector antenna is determined at that of the feeder antenna, then broadband feeder antenna, such as horn antennas [31], LPDAs [32], and eleven antennas [33] can be employed to the feeder antenna of the reflector. Therefore, to achieve broadband characteristics, the quad-ridge horn antenna is employed to the feeder antenna of the proposed antenna, as shown in Figure 7(a). The measured reflection coefficient of the feeder antenna is lower than −10 dB from 2 GHz to 7 GHz, which is in good agreement with the simulation results, as shown in Figure 7(b). This indicates that the proposed antenna has a broadband characteristic for various communication systems.

Figure 8 shows the reflectivity of the SUS mesh used as the reflective surface in the fabricated antenna. This reflectivity differs from that of the gold-coated molybdenum mesh used in the optimization. To compare the electrical characteristics of the proposed antenna between measurement and simulation, the reflectivity of the SUS mesh is measured at 3 GHz. A mesh with the same opening per inch (OPI) and reflectivity at 3 GHz is then modeled in the EM simulator, and its reflectivity is derived from 2 GHz to 6 GHz. The electrical characteristics of the proposed antenna are analyzed by applying this reflectivity to the reflector's surface in the simulation.

Figure 9 shows the deployment test of the proposed antenna. Using the CFRP properties, each rib can be wrapped around the center hub when the reflector is stowed in the rocket payload and returned to its deployed shape at the operating altitude. To verify the feasibility of mechanical characteristic, the deployment process of the proposed antenna is investigated using a dynamic simulation tool LS-Dyna [34], as shown in Figure 9(a). When the geometrical parameters (rib's thickness and height) and material properties (density, Young's modulus, and Poisson's ratio) are applied to the modeled ribs in LS-Dyna, the ribs can be wrapped into a compact circular shape and automatically deploy without damage and deformation, as shown in Figure 9(b). In addition, the deployment test of the proposed antenna is conducted, as shown in Figures 9(c), 9(d), and 9(e). Figure 9(c) represents a photograph of the stowed shape, which has a diameter of 0.2 m and a height of 0.26 m. When the constraining forces are removed from the stowed shape, the ribs return to their original shape, as shown in Figure 9(d). The ribs then are arranged perpendicularly to the center hub through spring hinges and column stoppers, as shown in Figure 9(e). The deployed shape has a diameter of 1.5 m and a height of 0.26 m, which means that the fabricated model has a deployment volume of 0.585 m^3(1.5 m × 1.5 m × 0.26 m) and a stowed volume of 0.0104 m^3(0.2 m × 0.2 m × 0.26 m), thus achieving a volume-reduction efficiency of 98.22%.

Figure 10 illustrates the measurement setup of the proposed antenna. In the measurement environment on Earth, the ribs can be bent by gravity, unlike in the zero-gravity environment at the satellite's operating altitude. Therefore, to measure the electrical characteristics of the proposed

TABLE 4. Mechanical parameters of the curved rib in LS-Dyna.

Parameters	Values
Density	1.2 g/cm^3
Young's modulus (elasticity)	120 GPa
Poisson's ratio	0.35

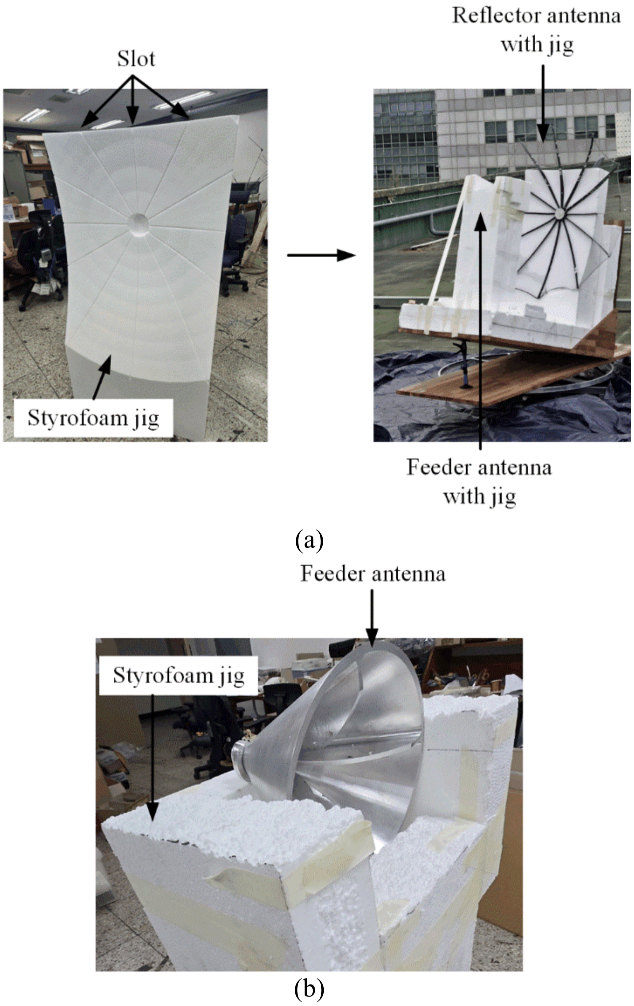

FIGURE 10. Measurement setup of the proposed antenna. (a) Styrofoam jig of reflector for zero-gravity. (b) Styrofoam jig of feeder antenna.

antenna, an environment similar to zero-gravity conditions should be implemented in the measurement setup. To address this issue, the fabricated mesh reflector is mounted on a Styrofoam jig ($\varepsilon_r = 1.1$, $\tan\delta = 0.0005$) with slots to support the curved ribs and the center hub, as shown in Figure 10(a). The feeder antenna is also mounted on the Styrofoam jig, as shown in Figure 10(b).

Figure 11 presents the measurement setup and 2-D radiation patterns of the proposed antenna in the near-field environment. To verify the electrical characteristic of the proposed antenna, the near-field is measured, as shown in Figure 11(a). In this measurement environment, the

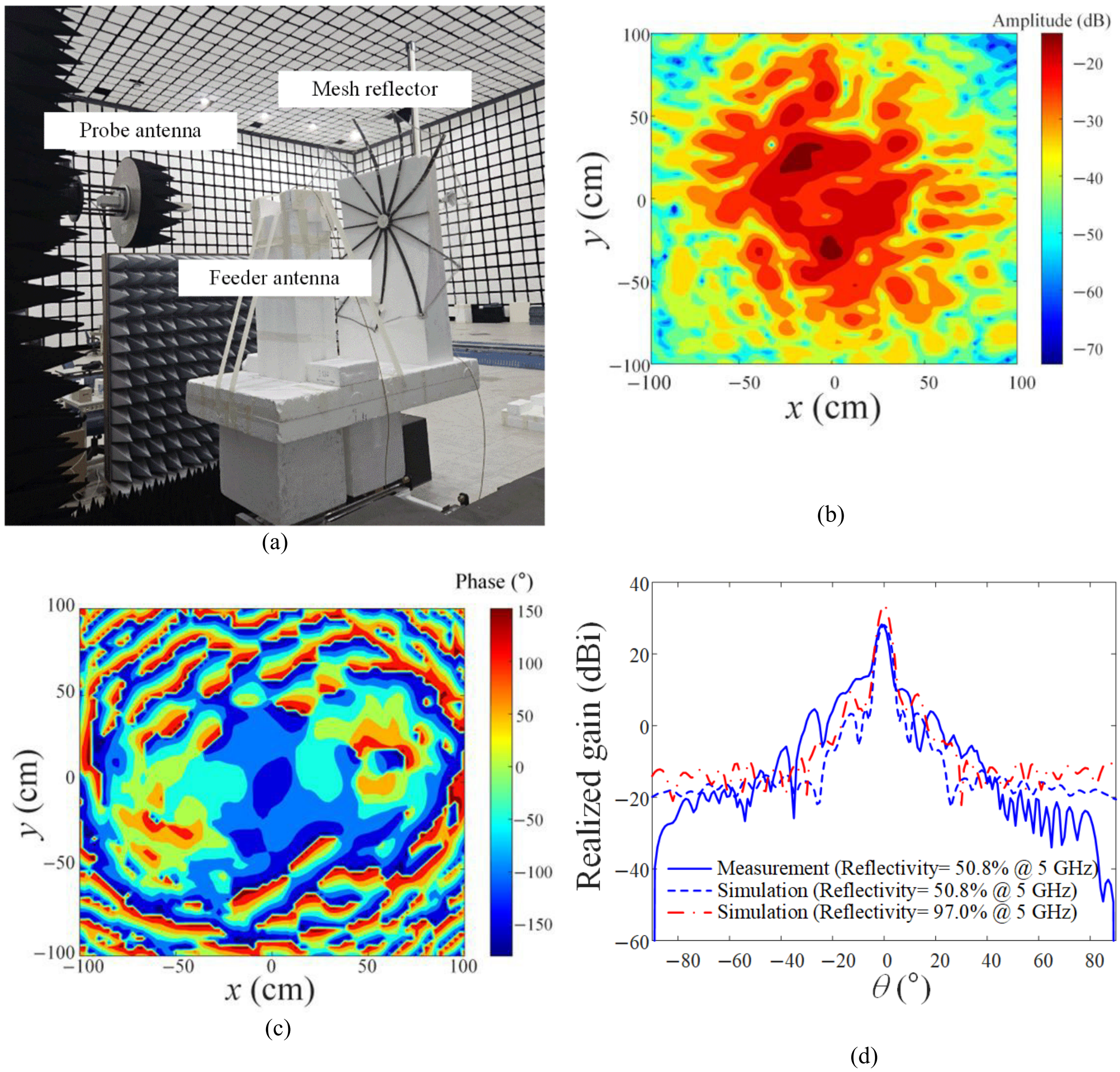

FIGURE 11. Measurement of the proposed antenna in the near-field environment. (a) Measurement setup. (b) Amplitude distribution of the near-field. (c) Phase distribution of the near-field. (d) 2-D radiation patterns.

bore-sight direction of the measured antenna is determined as the point, in which the measured phase distribution is bilateral symmetry in both the vertical and horizontal directions. A waveguide probe operating at 5 GHz scans over a range of 2 m × 2 m with a step size of 2.5 cm, and the amplitude and phase distributions of the near-field are measured, as shown in Figures 11(b) and 11(c). Thus, these measured near-field results are transformed into radiation patterns using the Near-Field To Far-Field (NF2FF) transformation [35]. Figure 11(d) shows the 2-D radiation patterns of the proposed antenna, where the solid and dashed lines indicate the measured and simulated results, respectively. At 5 GHz, the measured bore-sight gain and HPBW are 28.2 dBi and 3.7°, which agree well with the simulated results of 28.1 dBi and 4.5°, respectively. Since the SUS mesh is employed as the proposed mesh reflector antenna instead of the gold-coated molybdenum mesh, these results show a 5.7 dB decrease compared to the gain of 33.9 dBi obtained when a gold-coated molybdenum mesh is used. This reduction closely matches the reflectivity difference between the SUS mesh and the gold-coated molybdenum mesh when converted to the dB scale (−5.8 dB). This indicates that the proposed antenna can achieve a similar performance to that of the simulation result (red dotted dashed line) when a high reflectivity conducting mesh, such as the gold-coated molybdenum mesh, is applied to the proposed reflector antenna.

Figure 12 shows the measurement setup and results of the proposed antenna in the far-field environment. In the

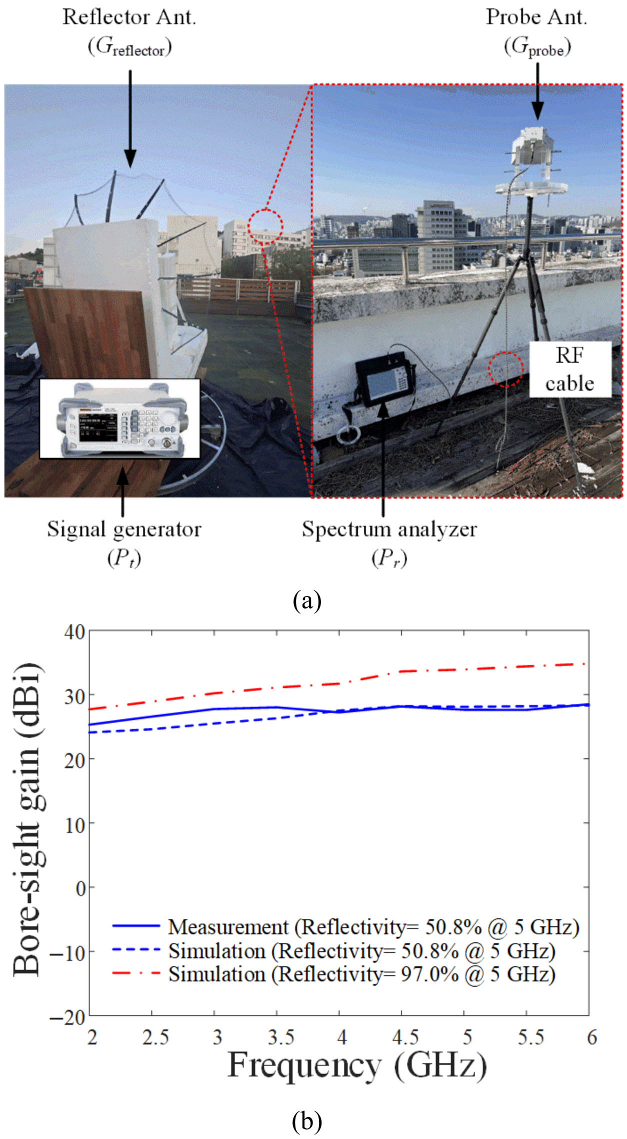

FIGURE 12. Measurement of the proposed antenna in the far-field environment. (a) Measurement setup. (b) Bore-sight gains.

near-field measurement, bore-sight gains and radiation patterns are derived using the NF2FF transformation. To verify these results, the bore-sight gains of the proposed antenna are measured in the far-field environment, as shown in Figure 12(a). For the far-field condition, the distance between the proposed antenna and the probe antenna is set to approximately 120 m. In this measurement setup, a signal generator is connected to the feeder antenna of the proposed antenna to supply the transmitted power. The probe antenna is placed in the bore-sight direction of the proposed antenna and is connected to a spectrum analyzer to measure the received power. The bore-sight gain of the proposed antenna is calculated using the Friis equation based on the measured transmitted/received power ratio, as shown in equations (1) and (2).

$$G_{\text{reflector}} = P_r - P_t - L_p - L_s - G_{\text{probe}} \tag{1}$$

TABLE 5. Far-field measurement parameters.

Parameters	Descriptions (unit)
$G_{\text{reflector}}$	Bore-sight gain of the reflector antenna (dBi)
G_{probe}	Bore-sight gain of the probe antenna (dBi)
P_t	Transmitted power (dBm)
P_r	Received power (dBm)
L_s	System loss (dB)
L_p	Path loss (dB)

$$L_p = 20\log_{10}\left(\frac{\lambda}{4\pi d}\right) \tag{2}$$

where G_{probe} refers to the bore-sight gains of the probe horn antenna, which has a minimum bore-sight gain of 10.23 dBi over measurement frequency range. The signal generator supplies transmitted power (P_t) of 16 dBm to the feeder antenna of the proposed antenna, while the spectrum analyzer connected with the probe horn antenna receives the power (P_r) transmitted by the proposed antenna. Considering the measurement environment, system loss (L_s) and path loss (L_p) are compensated. The system loss (L_s), which is presented over −6 dB at operating frequency, includes losses from various components in the measurement setup, such as RF cables, connectors, the signal generator, and the spectrum analyzer. The path loss (L_p) is calculated using the wavelength λ and the measurement distance at the operating frequency to equation (2). Therefore, various values are applied to equation (1), and the bore-sight gain of the proposed antenna ($G_{\text{reflector}}$) is calculated. Figure 12(b) shows the bore-sight gain of the proposed antenna, where the solid and dashed lines indicate the measured and simulated results, respectively. From 2 GHz to 6 GHz, the measured average bore-sight gain and aperture efficiency are 27.4 dBi and 18.1%, respectively, which agrees well with the simulated results of 26.7 dBi and 14.4%. Since the SUS mesh is employed to the proposed mesh reflector antenna instead of the gold-coated molybdenum mesh, these results indicate a 4.4 dB decrease compared to the average bore-sight gain of 31.8 dBi obtained when a gold-coated molybdenum mesh is used. This reduction closely matches the average reflectivity difference between the SUS mesh and the gold-coated molybdenum mesh when converted to the dB scale (−5.1 dB). This indicates that the proposed antenna can achieve similar performance to the simulation result (red dotted dashed line) when high reflectivity conducting mesh, such as the gold-coated molybdenum mesh, is applied to the fabrication.

IV. CONCLUSION

In this paper, we proposed a wrapped rib mesh reflector antenna with spring hinges and column stoppers for a high precision reflector surface. To achieve a high precision surface, twelve spring hinges and column stoppers were employed on the center hub, and curved ribs were connected to each spring hinge. The curved ribs were designed based on the parabola equation and were made of CFRP, which had lightweight, high elasticity, and flexibility, enabling the ribs to be wrapped into a compact circular shape around the center hub. A conducting mesh with high reflectivity was attached to the upper surface of the deployable structure. When the satellite reached its operating altitude, the wrapped ribs automatically deployed due to the elasticity of the CFRP and spring hinges, resulting in the attached mesh reforming into a parabolic shape. During deployment, the ribs were constrained by column stoppers, arranging them perpendicular to the center hub. In this configuration, the mesh could form a parabolic shape consistent with the parabola equation used in the design of the curved ribs. Therefore, the proposed mesh reflector could form a high precision reflector surface. Moreover, when the reflector was stowed in the rocket payload, the diameter of the reflector was reduced from 1.5 m to 0.2 m, and the height was maintained at 0.26 m. This meant that the fabricated model had a deployment volume of 0.585 m^3 (1.5 m × 1.5 m × 0.26 m) and a stowed volume of 0.0104 m^3 (0.2 m × 0.2 m × 0.26 m), thus achieving the volume-reduction efficiency of 98.22%. To verify the electrical characteristic of the proposed antenna, the bore-sight gains of the proposed antenna were measured in the far-field environment. The measured average bore-sight gain and aperture efficiency from 2 GHz to 6 GHz were 27.4 dBi and 18.1%, respectively, which agrees well with the simulated results of 26.7 dBi and 14.4%. Since the SUS mesh was employed as the proposed mesh reflector antenna instead of the gold-coated molybdenum mesh, these results indicated a 4.4 dB decrease compared to the average bore-sight gain of 31.8 dBi obtained when a gold-coated molybdenum mesh was used. This reduction closely matched the reflectivity difference between the SUS mesh (50.8%) and the gold-coated molybdenum mesh when converted to the dB scale (−5.1 dB). This indicates that the proposed antenna could achieve similar performance to the simulation result when a high reflectivity conducting mesh, such as the gold-coated molybdenum mesh, was applied to fabrication.

REFERENCES

[1] M. A. Imran, M. Zennaro, O. R. Popoola, L. Chiaraviglio, H. Zhang, P. Manzoni, J. van de Beek, R. Stewart, M. A. Cox, L. L. Mendes, and E. Pietrosemoli, ''Exploring the boundaries of connected systems: Communications for hard-to-reach areas and extreme conditions,'' *Proc. IEEE*, vol. 112, no. 7, pp. 912–945, Jul. 2024.

[2] H. S. Dhillon, H. Huang, and H. Viswanathan, ''Wide-area wireless communication challenges for the Internet of Things,'' *IEEE Commun. Mag.*, vol. 55, no. 2, pp. 168–174, Feb. 2017.

[3] X. Li, W. Feng, J. Wang, Y. Chen, N. Ge, and C.-X. Wang, ''Enabling 5G on the ocean: A hybrid satellite-UAV-terrestrial network solution,'' *IEEE Wireless Commun.*, vol. 27, no. 6, pp. 116–121, Dec. 2020.

[4] H. Li, J. Xu, S. Wu, and Q. Chen, ''Omnidirectional circularly polarized base station antenna with high gain and wide band,'' *Microw. Opt. Technol. Lett.*, vol. 66, no. 5, p. 34182, May 2024.

[5] M. Farasat, D. N. Thalakotuna, Z. Hu, and Y. Yang, ''A review on 5G sub-6 GHz base station antenna design challenges,'' *Electronics*, vol. 10, no. 16, p. 2000, Aug. 2021.

[6] H. Huang, Y. Liu, and S. Gong, ''A novel dual-broadband and dual-polarized antenna for 2G/3G/LTE base stations,'' *IEEE Trans. Antennas Propag.*, vol. 64, no. 9, pp. 4113–4118, Sep. 2016.

[7] A. Akinbolati, M. O. Ajewole, A. T. Adediji, and J. S. Ojo, ''Propagation curves and coverage areas of digital terrestrial television base stations in the tropical zone,'' *Heliyon*, vol. 6, no. 3, Mar. 2020, Art. no. e03599.

[8] M. A. Rupar, E. Larsen, H. B. Saglam, J. A. Savin, B. Gurdil, T. A. Lampe, N. Bruck, S. Peltotalo, and R. B. Blasco, ''Airborne beyond line-of-sight communication networks,'' *IEEE Commun. Mag.*, vol. 58, no. 8, pp. 34–39, Aug. 2020.

[9] Z. Xiao, J. Yang, T. Mao, C. Xu, R. Zhang, Z. Han, and X.-G. Xia, ''LEO satellite access network (LEO-SAN) toward 6G: Challenges and approaches,'' *IEEE Wireless Commun.*, vol. 31, no. 2, pp. 89–96, Apr. 2024.

[10] P. Tedeschi, S. Sciancalepore, and R. Di Pietro, ''Satellite-based communications security: A survey of threats, solutions, and research challenges,'' *Comput. Netw.*, vol. 216, Oct. 2022, Art. no. 109246.

[11] F. Vatalaro, G. E. Corazza, C. Caini, and C. Ferrarelli, ''Analysis of LEO, MEO, and GEO global mobile satellite systems in the presence of interference and fading,'' *IEEE J. Sel. Areas Commun.*, vol. 13, no. 2, pp. 291–300, Aug. 1995.

[12] Z. N. Chen, X. Qing, X. Tang, W. E. I. Liu, and R. Xu, ''Phased array metantennas for satellite communications,'' *IEEE Commun. Mag.*, vol. 60, no. 1, pp. 46–50, Jan. 2022.

[13] Y. Rahmat-Samii and R. Haupt, ''Reflector antenna developments: A perspective on the past, present and future,'' *IEEE Antennas Propag. Mag.*, vol. 57, no. 2, pp. 85–95, Apr. 2015.

[14] SpaceX. (Feb. 2025). *Falcon Heavy Rocket*. [Online]. Available: https://www.spacex.com/vehicles/falcon-heavy/

[15] D. Wu, M. Wu, P. Xiang, and Z. Yan, ''Surface accuracy analysis and optimization design of rib-mesh paraboloidal antenna reflectors,'' *Aerosp. Sci. Technol.*, vol. 129, Oct. 2022, Art. no. 107817.

[16] C. Im, W. Seo, S. Park, K. Kim, S. Park, and H. Choo, ''Design of a deployable broadband mesh reflector antenna for a SIGINT satellite system considering surface shape deformation,'' *Sensors*, vol. 24, no. 2, p. 384, Jan. 2024.

[17] N. Chahat, R. E. Hodges, J. Sauder, M. Thomson, E. Peral, and Y. Rahmat-Samii, ''CubeSat deployable Ka-band mesh reflector antenna development for Earth science missions,'' *IEEE Trans. Antennas Propag.*, vol. 64, no. 6, pp. 2083–2093, Jun. 2016.

[18] J.-S. Choi, T.-Y. Park, B.-G. Chae, and H.-U. Oh, ''Development of lightweight 6 m deployable mesh reflector antenna mechanisms based on a superelastic shape memory alloy,'' *Aerospace*, vol. 11, no. 9, p. 738, Sep. 2024.

[19] S. Morterolle, B. Maurin, J. Quirant, and C. Dupuy, ''Numerical form-finding of geotensoid tension truss for mesh reflector,'' *Acta Astronautica*, vol. 76, pp. 154–163, Jul. 2012.

[20] R. Nie, B. He, S. Yan, and X. Ma, ''Optimization design method for mesh reflector antennas considering the truss deformation and thermal effects,'' *Eng. Struct.*, vol. 208, Apr. 2020, Art. no. 110253.

[21] R. E. Freeland and G. Bilyeu, ''In-step inflatable antenna experiment,'' *Acta Astronautica*, vol. 30, pp. 29–40, Jul. 1993.

[22] M. Chandra, S. Kumar, S. Chattopadhyaya, S. Chatterjee, and P. Kumar, ''A review on developments of deployable membrane-based reflector antennas,'' *Adv. Space Res.*, vol. 68, no. 9, pp. 3749–3764, Nov. 2021.

[23] H. Zhang, M. Wu, P. Xiang, D. Wu, Z. Yan, and Q. Cui, ''Design, analysis, and test of an ultra-compact X-band deployable wrap-rib antenna,'' *Acta Astronautica*, vol. 228, pp. 918–930, Mar. 2025.

[24] S. Jiang, J. Wang, Q. Sui, and Q. Ye, ''Measurement of CFRP elastic modulus based on FBG reflectance spectrum analysis,'' *Measurement*, vol. 77, pp. 240–245, Jan. 2016.

[25] Dassault Systémes. (Feb. 2025). *CST Studio*. [Online]. Available: http://www.cst.com

[26] Y. Zhang, Y. Li, J. Zhang, J. Pan, L. Zhang, F. Tan, H. Wei, and W. Zhang, ''High-temperature effect on the tensile mechanical properties of unidirectional carbon fiber-reinforced polymer plates,'' *Materials*, vol. 14, no. 23, p. 7214, Nov. 2021.

[27] F. Xijun, Z. Yuege, and N. Tigang, ''Analysis of optical fiber performance at extreme temperature in low Earth orbit,'' *Optik*, vol. 250, Jan. 2022, Art. no. 168344.

[28] C. A. Balanis, *Antenna Theory: Analysis and Design*, 3rd ed., Hoboken, NJ, USA: Wiley, 2016.

[29] S. S. Siddesh, R. Harisankar, and G. K. Ananthasuresh, ''Surface profile accuracy of deployable mesh reflectors based on focal offset,'' in *Proc. iNaCoMM*, 2021, pp. 1355–1365.

[30] L. Zhang, Z. Wei, L. Wang, X. Yuan, H. Wu, and W. Xu, "Spectrum sharing in the sky and space: A survey," *Sensors*, vol. 23, no. 1, p. 342, Dec. 2022.
[31] N. Lee, C. Im, S. Park, and H. Choo, "Design of a metal 3D printed double-ridged horn antenna with stable gain and symmetric radiation pattern over a wide frequency range," *IEEE Access*, vol. 11, pp. 100565–100572, 2023.
[32] J. Park, C. Im, and H. Choo, "Design of a koch-curved LPDA antenna with optimized beamwidth to improve the aperture efficiency of reflector antennas," *IEEE Access*, vol. 13, pp. 106747–106758, 2025.
[33] J. Yang, M. Pantaleev, P.-S. Kildal, B. Klein, Y. Karandikar, L. Helldner, N. Wadefalk, and C. Beaudoin, "Cryogenic 2–13 GHz eleven feed for reflector antennas in future wideband radio telescopes," *IEEE Trans. Antennas Propag.*, vol. 59, no. 6, pp. 1918–1934, Jun. 2011.
[34] Ansys. (Feb. 2025). *LS-Dyna*. [Online]. Available: https://lsdyna.ansys.com
[35] Y. Gu, H.-H. Sun, and D. W. van der Weide, "A near-field super-resolution network for accelerating antenna characterization," *IEEE Trans. Antennas Propag.*, vol. 73, no. 3, pp. 1732–1742, Mar. 2025.

EN-YEAL YIM received the B.S. degree in electronic and electrical engineering from Hongik University, Seoul, South Korea, in 2022, where she is currently pursuing the Ph.D. degree in electronic and electrical engineering. His research interests include array antennas, radar antennas, and antennas.

CHANGHYEON IM received the B.S. degree in electronic and electrical engineering from Hongik University, Seoul, South Korea, in 2021, where he is currently pursuing the Ph.D. degree in electronic and electrical engineering. His research interests include mesh reflector antenna, 5G application, wireless power transfer, and ultra-wideband antenna.

HOSUNG CHOO (Senior Member, IEEE) received the B.S. degree in radio science and engineering from Hanyang University, Seoul, South Korea, in 1998, and the M.S. and Ph.D. degrees in electrical and computer engineering from The University of Texas at Austin, in 2000 and 2003, respectively. In September 2003, he joined the School of Electronic and Electrical Engineering, Hongik University, Seoul, where he is currently a Professor. His principal areas of research interests include electrically small antennas for wireless communications, reader and tag antenna for RFID, on-glass and conformal antennas for vehicles and aircraft, and array antenna for GPS applications.